NEOPLASIA
www.neoplasia.com

Volume 15 Number 4 April 2013 pp. 399–408 399

Methylation Profiling Defines an Extensive Field Defect in Histologically Normal Prostate Tissues Associated with Prostate Cancer[1,2]

Bing Yang*, Sachin Bhusari*, Jessica Kueck*, Pushpa Weeratunga*, Jennifer Wagner*, Glen Leverson†, Wei Huang‡,§ and David F. Jarrard*,‡,¶

*University of Wisconsin School of Medicine and Public Health, Madison, WI; †Department of Surgery, University of Wisconsin School of Medicine and Public Health, Madison, WI; ‡University of Wisconsin Carbone Comprehensive Cancer Center, Madison, WI; §Pathology and Laboratory Medicine, University of Wisconsin, Madison, WI; ¶Environmental and Molecular Toxicology, University of Wisconsin, Madison, WI

Abstract

Prostate cancer (PCa) is typically found as a multifocal disease suggesting the potential for molecular defects within the morphologically normal tissue. The frequency and spatial extent of DNA methylation changes encompassing a potential field defect are unknown. A comparison of non–tumor-associated (NTA) prostate to histologically indistinguishable tumor-associated (TA) prostate tissues detected a distinct profile of DNA methylation alterations (0.2%) using genome-wide DNA arrays based on the Encyclopedia of DNA Elements 18 sequence that tile both gene-rich and poor regions. Hypomethylation (87%) occurred more frequently than hypermethylation (13%). Several of the most significantly altered loci (*CAV1*, *EVX1*, *MCF2L*, and *FGF1*) were then used as probes to map the extent of these DNA methylation changes in normal tissues from prostates containing cancer. In TA tissues, the extent of methylation was similar both adjacent (2 mm) and at a distance (>1 cm) from tumor foci. These loci were also able to distinguish NTA from TA tissues in a validation set of patient samples. These mapping studies indicate that a spatially widespread epigenetic defect occurs in the peripheral prostate tissues of men who have PCa that may be useful in the detection of this disease.

Neoplasia (2013) 15, 399–408

Introduction

"Field cancerization" and "field defect" were terms first used in head and neck tumors to describe an increased frequency of cancer development found outside the visible boundaries of the primary tumor [1]. In the modern era, this definition has been refined to include genetically or epigenetically compromised cells identified in histologically normal appearing tissues. A field defect has been identified in gastric, colorectal, bladder, and esophageal cancers [2–4]. Epigenetic alterations limited solely to the immediate peritumor environment suggest a response of the surrounding tissue to the primary cancer. Single-gene epigenetic studies have identified these changes in a subset of specimens adjacent to the primary prostate cancers (PCa) [5–7]. Greater controversy exists whether widespread epigenetic alterations arise within the susceptible peripheral zone of the prostate that might underlie the regional multifocality at diagnosis, as well as the increased incidence with aging [8].

PCa development and progression are driven by the interplay of genetic and epigenetic changes [9]. One important epigenetic process is the reversible methylation of cytosine at CpG dinucleotides, a sequence underrepresented in the genome except at CpG islands

Address all correspondence to: David F. Jarrard, MD, 7037 Wisconsin Institute for Medical Research, 1111 Highland Avenue, Madison, WI 53705. E-mail: jarrard@urology.wisc.edu

[1]This work was supported by the National Institutes of Health (No. 2R01CA097131; http://grants.nih.gov/grants/) and the John Livesey endowment. The authors have declared that no competing interests exist.

[2]This article refers to supplementary materials, which are designated by Tables W1 to W4 and Figures W1 and W2 and are available online at www.neoplasia.com.

Received 18 January 2013; Revised 11 February 2013; Accepted 13 February 2013

DOI 10.1593/neo.13280

[10]. DNA hypermethylation at gene promoters leads to gene silencing and has been observed in preneoplastic lesions and cancers [11,12]. A decrease in global methylation is a signature of neoplastic processes and a predisposition to chromosomal instability and cancer [13,14]. Demethylation of LINE-1 elements in normal colonic mucosa in patients with multiple colon cancers has recently suggested a role for demethylation in cancer predisposition associated with a field defect [4].

Herein, we used an immunocapture approach to enrich methylated DNA and combined this with DNA microarrays based on the Encyclopedia of DNA Elements (ENCODE) 18 sequence that query functional elements throughout gene regions and are not focused solely on CpG island promoter regions. We then used these loci to evaluate the extent of the field defect in histologically normal tissues from men with PCa. Our data support a spatially widespread change in DNA methylation throughout the peripheral prostate at multiple loci that has implications for the development of the disease as well as clinical treatment.

Materials and Methods

Tissue Samples and Histopathology

Samples termed non–tumor-associated (NTA; mean, 63; range, 55–81 years) were obtained from organ donation or cystoprostatectomy and had extensive histologic evaluation to rule out associated PCa. Tumor-associated (TA; mean, 61; range, 57–64 years) prostate tissues were obtained from patients who underwent radical prostatectomy for PCa. The clinical-pathologic characteristics for all samples used in these studies are presented (Table W1). A separate validation group consisting of 12 NTA (mean, 60; range, 55–70 years) and 11 TA (mean, 57; range, 51–67 years) samples were evaluated using quantitative pyrosequencing.

To define the relationship of methylation to tumor foci, histologic sections containing both cancer and normal regions were generated from 26 (mean, 58; range, 44–69 years) radical prostatectomy specimens. Microdissection was performed to obtain tumor (T) and normal tissue adjacent (2 mm) to tumor foci (TAA) and at a greater distance (10 mm, TAD) as described [15]. Additional histopathologic criteria for the TA and NTA samples included similar epithelial-to-stromal ratios and lack of inflammation. Prostate specimens were confirmed to have no tumor by both hematoxylin and eosin (H&E) staining in three dimensions using step sectioning and α-methylacyl-CoA expression. For AMACR analysis, RNA was extracted using an RNeasy Mini Kit (Qiagen, Valencia, CA), and 300 ng of RNA were reverse transcribed with Ominscript. Quantitative real-time polymerase chain reaction (PCR) for total AMACR was performed using primer sequences, as reported [16]. This study was approved by Institutional Review Boards at the University of Wisconsin-Madison and the University of Pittsburgh.

DNA Methylation Microarrays

Genomic DNA was isolated using the DNeasy Blood and Tissue Kit (Qiagen). Roche NimbleGen ENCODE HG18 DNA methylation arrays were used. These arrays contain 385,000 50mer oligonucleotides (probes) that cover elements such as protein-coding genes, transcription units, protein binding sites, conserved DNA elements, chromatin assembly and modification features, and single-nucleotide polymorphisms. Notably, the probes are placed at 60-bp intervals to include both CpG and non-CpG islands within gene bodies, promoters, as well as intergenic regions (UCSC Genome browser, http://genome.ucsc.edu/ENCODE/encode.hg18.html). All chromosomes are represented on the arrays with the exception of 3 and 17.

Sample preparation for the microarray was performed following the manufacturer's protocol as previously detailed [11]. Briefly, 2 to 6 μg of high-quality genomic DNA was digested with *Mse*I (New England Biolabs, Ipswich, MA) to produce 200 to 1000 bp fragments (keeping CpG islands intact) and then heat denatured to form single strands. Methylated DNA fragments were immunoprecipitated (IP) with 1 μg of antibody against 5-methylcytidine (Abcam, Cambridge, MA) and captured with agarose beads. The DNA/antibody/bead mixture was digested with Proteinase K and purified with phenol-chloroform. Enrichment of the methylated IP DNA was validated with PCR primers for the H19-ICR specific for methylated DNA and FLJ25439 specific for unmethylated regions as described [17]. The labeling of IP and input DNA, microarray hybridization, and scanning were performed by NimbleGen Laboratories (Reykjavik, Iceland) as described [18]. Data were extracted from scanned images by using NimbleScan 2.4 extraction software (NimbleGen Systems, Inc, Madison, WI). The samples were assayed in duplicate.

Quantitative Pyrosequencing

Sodium bisulfite modification of genomic DNA was performed using the EpiTect Bisulfite Kit (Qiagen). Bisulfite-modified DNA was then amplified using PCR in preparation for pyrosequencing, with either the forward or reverse primer biotinylated [19]. All PCR and sequence primers for pyrosequencing were designed using PyroMark Assay Design 2.0 (Qiagen), and primer sequences are listed in Table W2*A*. The biotinylated PCR products were captured with streptavidin sepharose beads, denatured to single strand, and annealed to the sequencing primer for the pyrosequencing assay. *Sss*I methylase-treated bisulfite-converted DNA from human prostate epithelial cell and PPC1 were used as positive controls, and water substituted for DNA was used as a negative control. Methylation was quantified with the PyroMark MD Pyrosequencing System (Qiagen) within the linear range of the assay. All samples were analyzed by three independent experiments in duplicate.

Analysis of Methylation and Gene Expression

DNA and RNA were obtained from normal human prostate epithelial cells primary cultured from five patients and four human PCa cell lines (PC3, PPC1, Du145, and LNCaP). DNA methylation was evaluated by pyrosequencing as described above. Gene expression was measured by reverse transcription–quantitative PCR (RT-QPCR) using a Bio-Rad CFX 96 Real-Time PCR System and SYBR Green PCR Master Mix (Applied Biosystems, Grand Island, NY) as described. Primer sequences are listed in Table W2*B*. mRNA levels of each gene were normalized to β-actin as ΔC_T. Experiments were performed in duplicate in three independent experiments; a *t* test was used to compare the PCa cells to the normal prostate epithelial cells.

Data Analysis

Scaled $\log_2$ ratio gene-finding format (GFF) file and *P* value GFF files provided by NimbleGen Systems, Inc were used for microarray analysis. The scaled $\log_2$ ratio is the ratio of the test sample to the input signal when co-hybridized to the array. Scaling was performed by subtracting the biweight mean for all array features. From the scaled $\log_2$ ratio data, a fixed-length window was placed around each consecutive probe and the one-sided Kolmogorov-Smirnov test was

applied to determine whether the probes had a significantly more positive distribution of intensity log ratios than those in the rest of array. The resulting score for each probe was the $-\log_{10} P$ value. The probe IDs were first chosen on the basis of a $-\log_{10}[P]$ value that ranged from 2 to 10 resulting in around 1000 probes on each chromosome and 18,101 probes in total. A statistical analysis comparing the $\log_2$ ratios between the NTA and TA groups for the probes was then determined using a *t* test ($P < .05$). We used the more appropriate standard *t* test or the Satterthwaite approximation *t* test, depending on testing for equal variances when evaluating these data. Significantly changed probes were clustered by Java MultiExperiment View (MEV 4.6.2) with unsupervised hierarchical clustering [20]. For quantitative pyrosequencing, the methylation at each CpG site was expressed as a percentage. A two-tailed *t* test was used to test for differences between groups; $P < .05$ was considered statistically significant.

Results

Distinct Patterns of DNA Methylation Define TA from NTA Prostate Tissues

To identify probes, we used 385,000 locus arrays based on the ENCODE18 sequences that densely tile a series of biologically significant regions in ~1% of the human genome. These arrays query

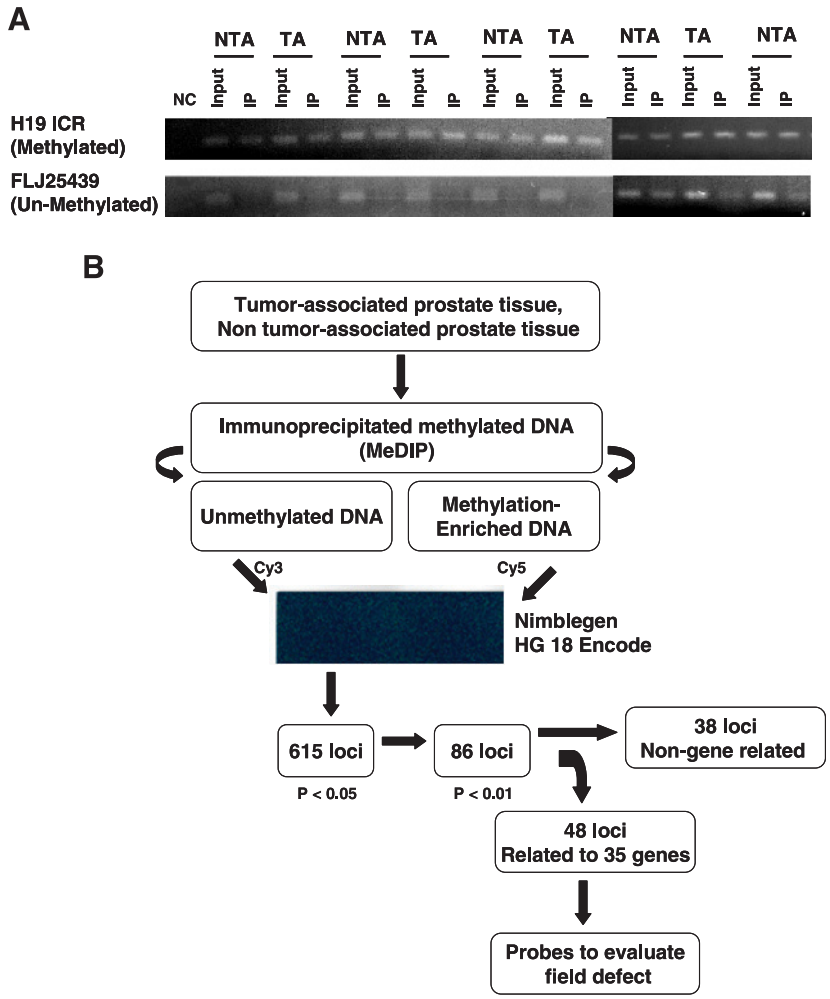

Figure 1. DNA methylation analysis using ENCODE18-based arrays of TA and NTA prostate tissues. (A) Verification of the IP for methylated DNA. Single-gene PCR was applied to both total genomic (Input) DNA and IP DNA before array analysis as described in Materials and Methods section. The H19 ICR served as a positive control for methylation and FLJ 25439 as a demethylation control. The IP shows lower demethylated levels. (B) Schema of methods. Genes aberrantly methylated in TA compared to NTA were identified by using an intensity cutoff ($-\log_{10}[P] = 2$–10), then a *t* test was used to compare the $\log_2$ ratios between groups. For further validation, statistical significance was used to rank the probes. (C) Genome-wide distribution of DNA methylation array differences at 385,000 loci in histologically normal TA prostate tissues compared to NTA tissues. Significant differences in methylation between TA and NTA prostate tissues were generated using a cutoff of probe score of $-\log_{10}[P] = 2$–10 and *t* test between two groups ($P < .05$). A total of 615 probes were differentially methylated in TA tissues with 537 demonstrating hypomethylation and 78 hypermethylation. The percentage (axis) is the significantly altered probe number *versus* the total probe number analyzed for each chromosome. Chromosomes 15 and 20 were differentially methylated to a greater extent than other chromosomes. (D) Heat map of significant DNA methylation array changes using unsupervised hierarchical clustering. Using more stringent criteria (*t* test, $P < .01$), 86 probes are shown comparing sets of NTA (left) to TA (right) and hierarchically ordered from top to bottom by relatively hypermethylation to hypomethylation. Green indicates relative hypomethylation, whereas the red shaded areas demonstrate hypermethylation of the TA set.

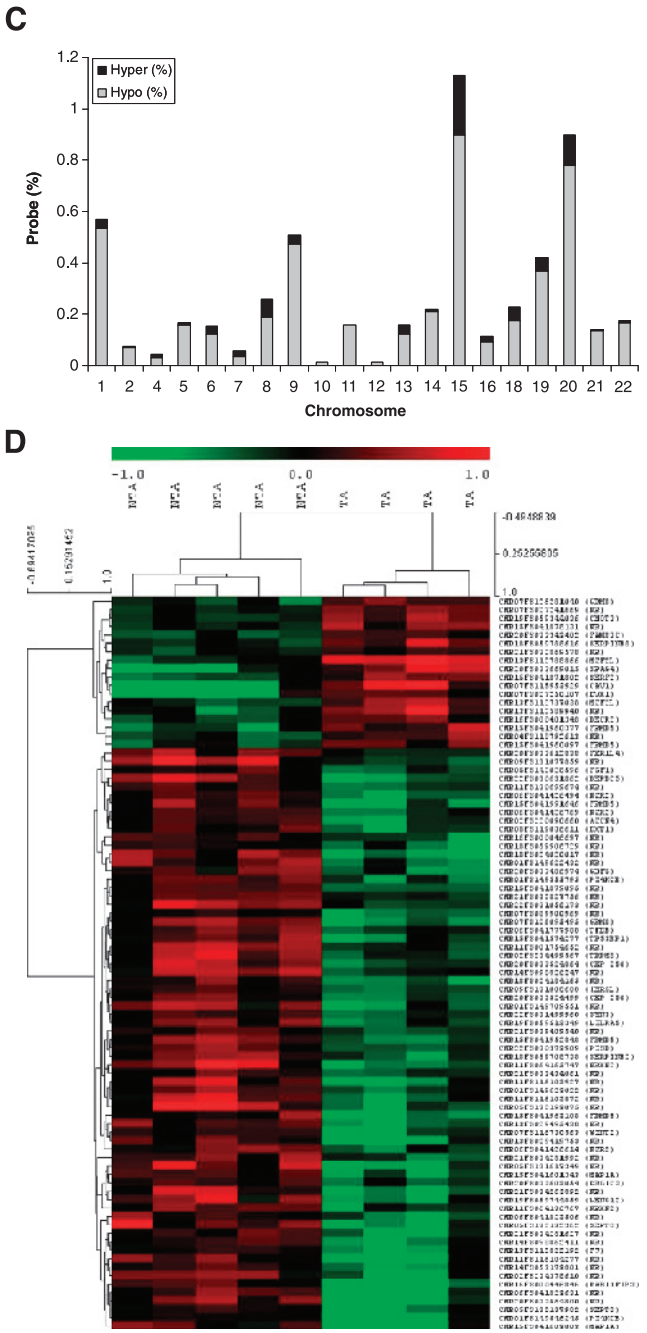

Figure 1. (*continued*).

functional elements throughout gene regions and are not focused solely on CpG island promoter regions. DNA was initially prepared in duplicate from four TA and five NTA prostate specimens, restriction digested, and enriched for methylated DNA by IP with an antibody against 5-methylcytidine, as described [11]. Peripheral zone prostate tissues were used for all of these studies as PCa demonstrates a predilection for this region.

To validate the IP, single-gene PCR was applied to confirm an enrichment of methylation in IP DNA compared to total genomic DNA (Input; Figure 1*A*). Total IP DNA and Input DNA were labeled with Cy5 and Cy3 dye, respectively, and then co-hybridized to the array (Figure 1*B*) [17]. There were 18,101 significant loci identified that were then statistically compared between TA and NTA tissue groups [21,22]. This generated 615 probes (0.16% of total) that were differentially methylated in TA tissues, of which 537 (87%) were hypomethylated and 78 (13%) were hypermethylated ($P < .05$; Figure 1*C*). Microarray data are available at http://www.ncbi.nlm.nih.gov/geo (Accession No. GSE38982).

Chromosome 15 demonstrated the greatest number of significantly differentially methylated probes (1.1%) in TA tissues, followed by chromosome 20 (0.9%). Across genomic regions, specific peaks were identified and defined as regions containing greater than two probes within a 500-bp length (Table W3*A*). From these results, we concluded that altered methylation between TA and NTA tissues occurs infrequently when using ENCODE-based genome arrays. Furthermore, arrays that query areas beyond promoter CpG islands reveal that

hypomethylation was more prevalent than increased methylation in tissues associated with tumors.

Identification of Probes for Analyzing the Field Defect in Prostate Specimens

To limit the number of loci for further study, more stringent statistical parameters ($P < .01$) were applied identifying 86 probes (Figure 1*B*). These probes were subjected to unsupervised hierarchical clustering using TMEV software to pictorially generate a heat map of methylation distinguishing TA from NTA prostate tissues (Figure 1*D*). Among these loci, 68 were hypomethylated and 18 were hypermethylated in TA tissues. Of these, 38 probes were not closely related to genes (Table W3*B*), and 48 were within 35 genes (Table 1). Loci associated with genes were primarily located within introns (78%) and were distant from transcription start sites.

Of the 48 gene-related probes (representing 35 genes), we evaluated 20 loci that demonstrated the most significant methylation changes on our arrays (Table 1). This included both hypermethylated and hypomethylated probes. In a separate set of 11 TA and 12 NTA prostate specimens, quantitative pyrosequencing was employed to validate these DNA methylation differences [19]. Because of technical reasons (mainly high CG density and mispriming; both limitations of pyrosequencing), we were unable to generate functional primers that covered 11 loci. *NCR2*, *WNT2*, and three others were not initially validated, although *NCR2* and *WNT2* were significantly altered in a high-grade disease subset (see below). We validated *CAV1*, *EVX1*, and *MCF2L* (hypermethylated) and *FGF1* (hypomethylated) in this tissue set (Figure 2*A*). The location of these four loci relative to gene structure is demonstrated in Figure 2*B*. These regions were downstream from the transcription start site and included both exonic and intronic regions making them less likely to alter gene

Table 1. Gene-related Loci Ranked by Significance.

Gene	Gene Name	Accession No.	Location	Hypermethylation or Hypomethylation	Distance to TSS	CpG Island	Gene Body	Exon/ Intron
*MCF2L**	Cell line derived transforming sequence-like	NM_024979	Chr13: 112,704,068–112,792,498	Hyper	+117331	Y	Y	Intron
*RAB11FIP3**	RAB11 family interacting protein 3	NM_014700	Chr16: 415,668–512,482	Hypo	+31178	Y	Y	Intron
CNOT3	CCR4-NOT transcription complex 3	BC016474	Chr19: 59,333,294–59,351,230	Hyper	+10789	Y	Y	Exon
*NCR2**	Natural cytotoxicity triggering receptor 2	AJ010100	Chr6: 41,411,566–41,426,579	Hypo	+14989	Y	Y	Exon
IER5L	Immediate early response 5-like	NM_203434	Chr9: 130,978,873–131,012,683	Hypo	–28327	N	N	–
SERF2	Small EDRK-rich factor 2	BC015491	Chr15: 41,871,834–41,873,536	Hyper	+15217	Y	Y	Exon
FRMD5	FERM domain containing 5	NM_032892	Chr15: 41,952,764–42,274,683	Hypo	+311563	N	Y	Intron
MCF2L	Cell line derived transforming sequence-like	NM_024979	Chr13: 112,704,068–112,792,498	Hyper	+65503	N	Y	Intron
FAM83C	Family with sequence similarity 83 C	NM_178468	Chr20: 33,336,947–33,343,639	Hyper	+189	Y	Y	Exon
FRMD5	FERM domain containing 5	NM_032892	Chr15: 41,952,764–42,274,683	Hypo	+321825	N	N	–
DEPDC5	DEP domain containing 5	AJ698951	Chr22: 30,480,852–30,632,599	Hypo	+151926	N	Y	Intron
*EVX1**	Even-skipped homeobox 1	NM_001989	Chr7: 27,248,945–27,252,717	Hyper	+1419	Y	Y	Intron
MAP1A	Microtubule-associated protein 1A	NM_002373	Chr15: 41,597,132–41,611,110	Hypo	+4246	Y	Y	Exon
*FGF1**	Fibroblast growth factor 1	NM_000800	Chr5: 141,953,305–142,045,812	Hypo	+29175	Y	Y	Intron
SYN3	Synapsin III	NM_003490	Chr22: 31,238,539–31,732,683	Hypo	+284369	N	Y	Intron
GRM8	Glutamate receptor, metabotropic 8	NM_000845	Chr7: 125,865,894–126,670,548	Hypo	+584116	N	Y	Intron
SERPINB8	Serpin peptidase inhibitor B8	BC034528	Chr18: 59,788,332–59,804,866	Hyper	+374	Y	Y	Intron
*CAV1**	Caveolin 1	AF 172085	Chr7: 115,953,642–115,986,904	Hyper	+1855	Y	Y	Exon
*WNT2**	Wingless-type MMTV integration site	BC 078170	Chr7: 116,704,514–116750565	Hypo	+19961	Y	Y	Intron
*CEP250**	Centrosomal protein	AF022655	Chr20: 33,511,231–33,563,123	Hypo	+17863	N	Y	Intron
*PI4KCB**	Phosphatidylinositol 4-kinase	NM_002651	Chr1: 149,531,036–149,565,348	Hypo	+11021	N	Y	Intron
PISD	Phosphatetidylserine decarboxylase	CR456540	Chr22: 30,345,379–30,388,195	Hypo	–13468	N	N	–
GRM8	Glutamate receptor, metabotropic 8	NM_000845	Chr7: 125,865,894–126,670,548	Hyper	+398576	N	Y	Intron
SPAG4	Sperm associated antigen 4	NM_003116	Chr20: 33,667,222–33,672,379	Hyper	+1793	Y	Y	Intron
NCR2	Natural cytotoxicity triggering receptor 2	AJ010100	Chr6: 41,411,566–41,426,579	Hypo	+15264	Y	N	–
FRMD5	FERM domain containing 5	NM_032892	Chr15: 41,952,764–42,274,683	Hypo	+293027	Y	Y	Intron
NRXN2	Neurexin 2	NM_138734	Chr11: 64,130,221–64,167,363	Hypo	+81441	N	Y	Intron
ACCN4	Amiloride-sensitive cation channel 4	NM_182847	Chr2: 220,087,295–220,111.738	Hypo	+3525	Y	Y	Intron
SERPINB2	Serpin peptidase inhibitor, B2	NM_002575	Chr18: 59,705,921–59,722,100	Hypo	+2820	N	Y	Intron
CEP250	Centrosomal protein	AF022655	Chr20: 33,511,231–33,563,123	Hypo	+18228	N	Y	Intron
FRMD5	FERM domain containing 5	NM_032892	Chr15: 41,952,764–42,274,683	Hyper	+314296	N	Y	Intron
FER1L4	Fer-1–like 4	AL833764	Chr20: 33,609,920–33,651,008	Hypo	+46003	N	Y	Intron
ERGIC3	ERGIC and golgi 3	AF116614	Chr20: 33,593,290–33,608,818	Hypo	+9863	Y	Y	Intron
TRPM8	Transient receptor potential cation channel	NM_024080	Chr2: 234,490,781–234,592,905	Hypo	+8786	N	Y	Intron
TFEB	Transcription factor EB	NM_007162	Chr6: 41,759,693–41,810,766	Hypo	+33939	Y	Y	Intron
SEPT8	Septin	AF440762	Chr5: 132,114,415–132,140,966	Hypo	+9050	Y	Y	Intron
EXT1	Exostoses 1	BC001174	Chr8: 118,880,782–119,192,632	Hypo	+156580	N	Y	Intron
GDF5	Growth differentiation factor 5	NM_000557	Chr20: 33,484,562–33,489,441	Hypo	+2409	N	Y	Intron
SEPT8	Septin	AF440762	Chr5: 132,114,415–132,140,966	Hypo	+3430	Y	Y	Intron
NRXN2	Neurexin 2	NM_138734	Chr11: 64,130,221–64,167,363	Hypo	+110421	Y	Y	Intron
TP53BP1	Tumor protein p53 binding protein 1	NM_005657	Chr15: 41,486,698–41,590,028	Hypo	+15672	N	Y	Intron
F7	Coagulation factor VII	NM_019616	Chr13: 112,808,105–112,822,346	Hypo	+14087	Y	Y	Exon
LILRA5	Leukocyte immunoglobulin-like receptor A5	NM_181985	Chr19: 59,510,164–59,516,221	Hypo	+2824	N	Y	Intron
DECR2	2,4-dienoyl CoA reductase 2	AK128012	Chr16: 391,893–402,371	Hyper	+9490	Y	Y	Intron
FRMD5	FERM domain containing 5	NM_032892	Chr15: 41,952,764–42,274,683	Hyper	+314576	N	Y	Intron
PI4KCB	Phosphatidylinositol 4-kinase	NM_002651	Chr1: 149,531,036–149,565,348	Hypo	+20522	N	Y	Intron
NCR2	Natural cytotoxicity triggering receptor 2	AJ010100	Chr6: 41,411,566–41,426,579	Hypo	+15109	Y	N	–
MAP1A	Microtubule-associated protein 1A	NM_002373	Chr15: 41,597,132–41,611,110	Hypo	+5906	Y	Y	Exon

*Probes subjected to validation using quantitative pyrosequencing. Of the initial 20 loci listed, 11 were not able to be assessed due to technical limitations regarding probe design and performance.

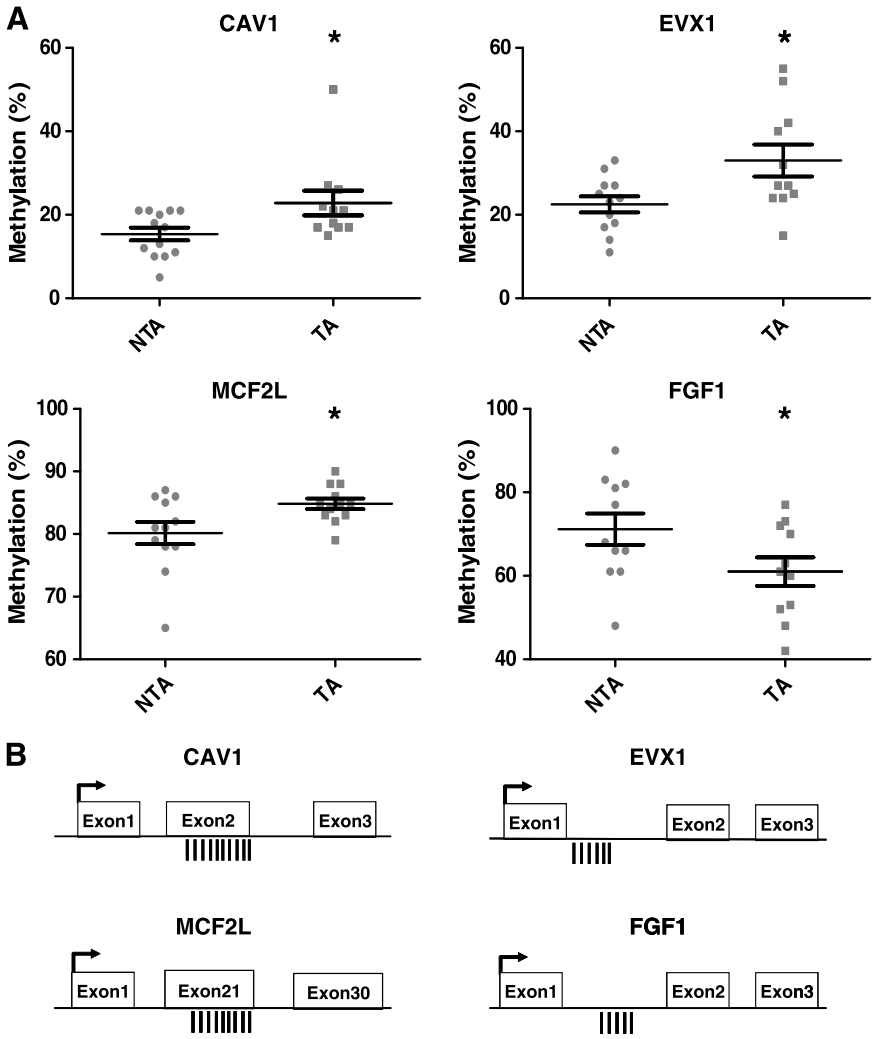

Figure 2. Validation of loci identified by DNA methylation array in additional prostate tissues using quantitative pyrosequencing. (A) Analysis of methylation was performed using quantitative pyrosequencing as described in Materials and Methods section. An additional validation set of NTA tissues (12) was compared to TA tissues (11). All loci shown were significantly altered in TA when compared to NTA samples ($P < .05$). (B) Location of selected loci within genes that were analyzed by quantitative pyrosequencing. Exon and intron boundaries are shown, as well as the transcription start site. The genome-wide analysis resulted in loci that were not typically located in promoter CpG islands. Tick marks represent CG sites analyzed.

expression. To evaluate this issue, we performed a correlation analysis for these four loci examining methylation and gene expression in a series of normal prostate epithelial cells (five) and PCa cell lines (four). Changes in methylation did not correlate with altered transcript expression from these four associated genes (Figure W2). The above data validated these four primer sets as tools marking an epigenetic field defect present in men with associated PCa that were then used in subsequent mapping experiments.

Identification of a Widespread Methylation Field Defect in the Peripheral Prostate

We then used these probes to test whether tissues adjacent to PCa tumor foci are preferentially altered, suggesting only an immediate peritumor response, or whether aberrant methylation occurs at a distance from the tumor indicating a more widespread field defect. The extent of the field defect was assessed using four differentially methylated markers in 26 additional histologically normal tissues from men with cancer. Clinical and pathologic information is presented (Table W1). We dissected normal tissues 2 mm adjacent (TAA) and compared these to tissue more than 10 mm distant (TAD) from the main tumor focus for each of these 26 specimens (Figure 3*A*). H&E staining of step sections was used to exclude contamination by tumor cells, significant inflammation, and the presence of high-grade prostatic intraepithelial neoplasia (PIN), a putative cancer precursor [23]. AMACR expression, a PCa marker, was determined by QPCR, and samples contaminated by overt cancer were removed (Figure W1).

When compared to NTA tissues, hypermethylation of probes associated with *CAV1*, *EVX1*, and *MCF2L* and hypomethylation of *FGF1* demonstrated significant changes in both adjacent (TAA), as well as distant tissues (Figure 3*B*). Results for each CpG tested are listed in Table W4. We noted no significant difference in the extent of methylation seen at different distances from the tumor using these unbiased probes. We also evaluated methylation in the associated tumor (T) for each sample. The methylation change representing the field defect was also present in the tumor samples at three loci. At *FGF1*, the tumor did not demonstrate hypomethylation similar

to the TA tissue, suggesting that these defects are not always enriched for in the associated tumors. In summary, similar methylation extent in both adjacent and distant tissues indicates that the epigenetic field defect in the prostate is spatially widespread and not localized solely to the immediate peritumor environment.

We also performed a subset analysis on TA tissues looking at these changes in intermediate (Gleason 5–7) or high-grade (Gleason 8–10) cancers. Two loci, *NCR2* and *WNT2*, that were not significantly altered when all tissue grades were examined were found to be significantly altered in the high-grade but not intermediate-grade subset (Figure 4*A*). The location of *NCR2* and *WNT2* relative to gene structure is demonstrated in Figure 4*B*. Other loci did not distinguish between the field defect associated with high- or low-grade disease. These data suggest that distinct field methylation alterations may be solely associated with the presence of high-grade cancer.

Discussion

Research has led to a proposal that a field defect may underlie the development of multifocal cancer [1]. Initial efforts in characterizing

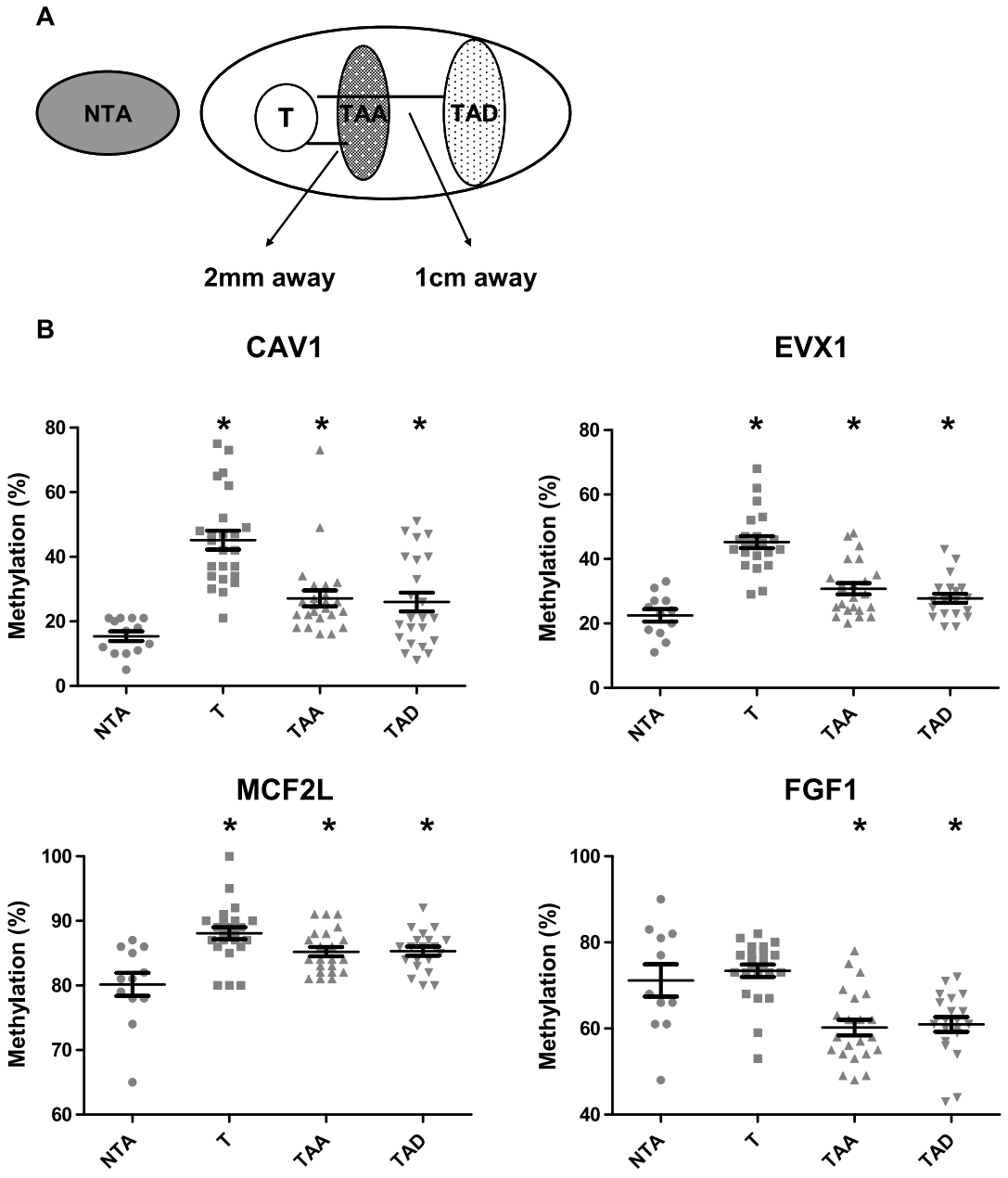

Figure 3. Analysis of extent of field defect in prostatectomy samples using identified probes. (A) Schematic showing prostate tumor (T) and adjacent (TAA) and distant (TAD) normal tissue dissection as well as NTA specimens. Radical prostatectomy samples containing tumor foci were sectioned and samples dissected for subsequent analyses. Adjacent and distant TA tissues did not contain histologic cancer. Samples were assessed three-dimensionally using step sectioning. (B) Analysis of methylation at differentially methylated loci in above dissected prostate tissues and NTA prostate tissues using quantitative pyrosequencing. Methylation analyses for *CAV1*, *EVX1*, *MCF2L*, and *FGF1* were significantly different when comparing T, TAA, or TAD to NTA (*$P < .05$). No significant erosion in methylation with increasing distances from the primary tumor was observed when TAA was compared to TAD. Technical replicates obtained from independent PCR reactions showed average SDs of 2.4% for *CAV1*, 1.5% for *EVX1*, 1.6% for *MCF2L*, and 2.1% for *FGF1*, respectively.

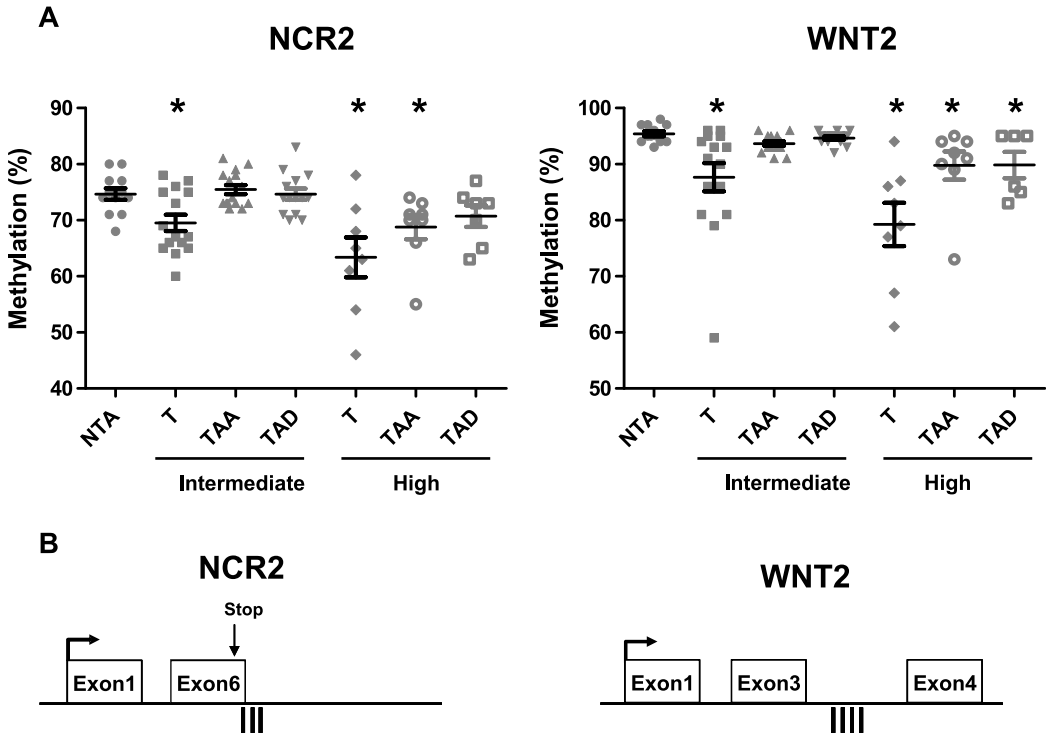

Figure 4. Analysis demonstrates a relationship between grade and methylation for several tested loci. (A) Quantitative pyrosequencing was performed on nine loci (Table 1). Prostate tumor (T), adjacent (TAA), and distant (TAD) tissues were divided into high- (Gleason score of 8–10) and intermediate- (Gleason score of 5–7) grade tissues. Tissues without associated cancer were also evaluated (NTA). *NCR2* and *WNT2* were found to only be significantly hypomethylated in TA tissues associated with the presence of high-grade cancer when compared to NTA ($P < .05$). (B) Location of *NCR2* and *WNT2* region where the probes are located.

this process focused on genetic alterations [24,25]. More recently, epigenetic changes have been proposed as an etiology [26,27]. In the current study, we used high-resolution genome-wide arrays that cover a range of biologically significant regions (not limited to promoter regions) to identify significant changes in DNA methylation that occur within histologically normal tissues associated with PCa. We validated several of these loci and used them as probes to demonstrate for the first time that methylation changes are spatially widespread and not restricted to the immediate peritumor environment as previously thought [2,4,15]. Finally, these methylation alterations permit a clear distinction between TA and NTA prostate tissues.

To date, epigenetic profiling of TA histologically normal tissues has not been performed in the prostate. Our genome-wide assessment of specific loci demonstrates that hypomethylation was seen more commonly than hypermethylation in TA prostate tissues. This surprising finding may be a result of using arrays that do not solely examine promoter CpG islands but densely assess gene-enriched regions, including intergenic regions, of the genome. The use of these arrays also explains the relatively low frequency of methylation changes (0.2%) found compared to studies in other cancers using CpG promoter arrays [28]. Hypomethylation was recently found at LINE-1 sequences in normal colonic mucosa of patients with multiple colon cancers, suggesting that demethylation may underlie the field defect found in these patients [4]. These findings were also increased with aging, and the authors proposed a "wear and tear" model to explain the propensity of colon cancer with aging [4]. In the prostate, DNA hypomethylation may be found in PIN [29], a cancer precursor. Our data that widespread hypomethylation occurs in the prostate field defect extend these findings and lead to speculation that epigenetic alterations in TA tissues may possibly precede the histologic changes of PIN and cancer.

A debate exists regarding whether the peripheral prostate may undergo widespread methylation changes similar to bladder cancer, a disease also characterized by multifocality and recurrence [27]. In bladder, there was no dependence on distance from the primary tumor. Previously, methylation studies using single genes *GSTP1*, *RASSF1A*, *APC*, and *RARβ2* altered in PCa identified methylation changes in a subset of specimens only adjacent to the primary tumor [5–7]. This suggested that methylation alterations were limited solely to the immediate peritumor environment in the prostate. In contrast, in the present epigenomic profiling study, we find that methylation alterations consistently extended even to regions distant (>1 cm) from tumor foci. A similar widespread field defect was demonstrated during evaluation of *insulin-like growth factor 2* loss of imprinting in peripheral prostate tissues [15]. Insulin-like growth factor 2 loss of imprinting is an age-related event in the human prostate that is associated with cancer formation [30]. This epigenetic association has also been seen in the colon and predisposes to cancer formation [31]. These data suggest a more widespread methylation change in the histologically normal peripheral prostate of men with cancer that we postulate predisposes the gland to multiple tumor formation with aging. Further research will be needed to address this hypothesis and how a widespread methylation field defect might arise, whether due to diet or environmental exposures [32,33].

Our primary goal was to use methylation arrays to define an unbiased panel of probes with which to evaluate whether a widespread

field defect occurs in PCa. Thus, we used a more limited number of samples initially and further validated a panel of genes with quantitative pyrosequencing. We found six of nine loci to be validated in our other tissue sets, indicating a false discovery rate of 33%. To select loci for validation, we used approaches commonly employed in gene array studies (e.g., statistical value) [11]. The majority of probes identified fell within CpG islands [34], but interestingly none fell into defined gene promoter regions (Table 1). Hypermethylation within promoters has been linked to decreased gene expression [35,36], but the function of CpG islands outside these regions remains uncertain. No correlation with expression and methylation was noted at the majority of these loci when normal and cancer cell lines were examined (Figure W2). At *NCR2* and *WNT2*, a correlation was seen between increased methylation and expression. Methylation within the gene bodies has been associated with elevated gene expression in genome-wide studies [37]. These changes may reflect alternate promoter usage that could impact expression in a sense or antisense manner. Alternatively, given the potential for long-range epigenetic silencing through chromatin looping, we postulate that the methylation changes identified may herald alterations in nuclear structure that influence gene expression at distant sites [38].

The current findings suggest a methylation field defect that may encompass peripheral prostate tissue, the susceptible region of the gland, even at a distance from the tumor. These findings have several additional implications. Several of the loci identified in this study were recently used as a test to successfully identify the presence of PCa elsewhere in the prostate solely from normal biopsy tissue in a group of clinical patients with an excellent area under the curve of 0.79 [39]. An additional finding of several regions that were associated only with high-grade cancer might suggest an early marker for more aggressive PCa. Finally, the assessment of alterations that occur in PCa have typically compared tumor to "normal" tissues within the same prostate gland. The current study indicates that histologically normal tissue from men who have PCa may already contain methylation abnormalities leading to an underestimation of epigenetic changes within the tumor.

References

[1] Slaughter DP, Southwick HW, and Smejkal W (1953). Field cancerization in oral stratified squamous epithelium; clinical implications of multicentric origin. *Cancer* **6**, 963–968.

[2] Maekita T, Nakazawa K, Mihara M, Nakajima T, Yanaoka K, Iguchi M, Arii K, Kaneda A, Tsukamoto T, Tatematsu M, et al. (2006). High levels of aberrant DNA methylation in *Helicobacter pylori*–infected gastric mucosae and its possible association with gastric cancer risk. *Clin Cancer Res* **12**, 989–995.

[3] Takahashi T, Habuchi T, Kakehi Y, Mitsumori K, Akao T, Terachi T, and Yoshida O (1998). Clonal and chronological genetic analysis of multifocal cancers of the bladder and upper urinary tract. *Cancer Res* **58**, 5835–5841.

[4] Kamiyama H, Suzuki K, Maeda T, Koizumi K, Miyaki Y, Okada S, Kawamura YJ, Samuelsson JK, Alonso S, Konishi F, et al. (2012). DNA demethylation in normal colon tissue predicts predisposition to multiple cancers. *Oncogene* **31**, 5029–5037.

[5] Aitchison A, Warren A, Neal D, and Rabbitts P (2007). RASSF1A promoter methylation is frequently detected in both pre-malignant and non-malignant microdissected prostatic epithelial tissues. *Prostate* **67**, 638–644.

[6] Hanson JA, Gillespie JW, Grover A, Tangrea MA, Chuaqui RF, Emmert-Buck MR, Tangrea JA, Libutti SK, Linehan WM, and Woodson KG (2006). Gene promoter methylation in prostate tumor-associated stromal cells. *J Natl Cancer Inst* **98**, 255–261.

[7] Henrique R, Jeronimo C, Teixeira MR, Hoque MO, Carvalho AL, Pais I, Ribeiro FR, Oliveira J, Lopes C, and Sidransky D (2006). Epigenetic heterogeneity of high-grade prostatic intraepithelial neoplasia: clues for clonal progression in prostate carcinogenesis. *Mol Cancer Res* **4**, 1–8.

[8] Miller GJ and Cygan JM (1994). Morphology of prostate cancer: the effects of multifocality on histological grade, tumor volume and capsule penetration. *J Urol* **152**, 1709–1713.

[9] Schulz WA and Hoffmann MJ (2009). Epigenetic mechanisms in the biology of prostate cancer. *Semin Cancer Biol* **19**, 172–180.

[10] Bird A (2002). DNA methylation patterns and epigenetic memory. *Genes Dev* **16**, 6–21.

[11] Morris MR, Ricketts CJ, Gentle D, McRonald F, Carli N, Khalili H, Brown M, Kishida T, Yao M, Banks RE, et al. (2011). Genome-wide methylation analysis identifies epigenetically inactivated candidate tumour suppressor genes in renal cell carcinoma. *Oncogene* **30**, 1390–1401.

[12] Wu YH, Tsai Chang JH, Cheng YW, Wu TC, Chen CY, and Lee H (2007). Xeroderma pigmentosum group C gene expression is predominantly regulated by promoter hypermethylation and contributes to p53 mutation in lung cancers. *Oncogene* **26**, 4761–4773.

[13] Eden A, Gaudet F, Waghmare A, and Jaenisch R (2003). Chromosomal instability and tumors promoted by DNA hypomethylation. *Science* **300**, 455.

[14] Feinberg AP and Vogelstein B (1983). Hypomethylation distinguishes genes of some human cancers from their normal counterparts. *Nature* **301**, 89–92.

[15] Bhusari S, Yang B, Kueck J, Huang W, and Jarrard DF (2011). Insulin-like growth factor-2 (IGF2) loss of imprinting marks a field defect within human prostates containing cancer. *Prostate* **71**, 1621–1630.

[16] Ouyang B, Leung YK, Wang V, Chung E, Levin L, Bracken B, Cheng L, and Ho SM (2011). α-Methylacyl-CoA racemase spliced variants and their expression in normal and malignant prostate tissues. *Urology* **77**, 249.e1–249.e7.

[17] Weber M, Davies JJ, Wittig D, Oakeley EJ, Haase M, Lam WL, and Schubeler D (2005). Chromosome-wide and promoter-specific analyses identify sites of differential DNA methylation in normal and transformed human cells. *Nat Genet* **37**, 853–862.

[18] Roche.NimbleGen (2010). *Arrays User's Guide DNA Methylation Arrays Version 7.2*.

[19] Tost J, El abdalaoui H, and Gut IG (2006). Serial pyrosequencing for quantitative DNA methylation. *Biotechniques* **40**, 721–722, 724, 726.

[20] Saeed AI, Bhagabati NK, Braisted JC, Liang W, Sharov V, Howe EA, Li J, Thiagarajan M, White JA, and Quackenbush J (2006). TM4 microarray software suite. *Methods Enzymol* **411**, 134–193.

[21] Ruike Y, Imanaka Y, Sato F, Shimizu K, and Tsujimoto G (2010). Genome-wide analysis of aberrant methylation in human breast cancer cells using methyl-DNA immunoprecipitation combined with high-throughput sequencing. *BMC Genomics* **11**, 137.

[22] Wilson IM, Davies JJ, Weber M, Brown CJ, Alvarez CE, MacAulay C, Schübeler D, and Lam WL (2006). Epigenomics: mapping the methylome. *Cell Cycle* **5**, 155–158.

[23] Ayala AG and Ro JY (2007). Prostatic intraepithelial neoplasia: recent advances. *Arch Pathol Lab Med* **131**, 1257–1266.

[24] Braakhuis BJ, Tabor MP, Kummer JA, Leemans CR, and Brakenhoff RH (2003). A genetic explanation of slaughter's concept of field cancerization. *Cancer Res* **63**, 1727–1730.

[25] Garcia SB, Park HS, Novelli M, and Wright NA (1999). Field cancerization, clonality, and epithelial stem cells: the spread of mutated clones in epithelial sheets. *J Pathol* **187**, 61–81.

[26] Hu M, Yao J, Cai L, Bachman KE, van den Brule F, Velculescu V, and Polyak K (2005). Distinct epigenetic changes in the stromal cells of breast cancers. *Nat Genet* **37**, 899–905.

[27] Wolff EM, Chihara Y, Pan F, Weisenberger DJ, Siegmund KD, Sugano K, Kawashima K, Laird PW, Jones PA, and Liang G (2010). Unique DNA methylation patterns distinguish noninvasive and invasive urothelial cancers and establish an epigenetic field defect in premalignant tissue. *Cancer Res* **70**, 8169–8178.

[28] Takamaru H, Yamamoto E, Suzuki H, Nojima M, Maruyama R, Yamano HO, Yoshikawa K, Kimura T, Harada T, Ashida M, et al. (2012). Aberrant methylation of RASGRF1 is associated with an epigenetic field defect and increased risk of gastric cancer. *Cancer Prev Res (Phila)* **5**, 1203–1212.

[29] Yang B, Sun H, Lin W, Hou W, Li H, Zhang L, Li F, Gu Y, Song Y, Li Q, et al. (2011). Evaluation of global DNA hypomethylation in human prostate cancer and prostatic intraepithelial neoplasm tissues by immunohistochemistry. *Urol Oncol*, E-pub ahead of print.

[30] Fu VX, Dobosy JR, Desotelle JA, Almassi N, Ewald JA, Srinivasan R, Berres M, Svaren J, Weindruch R, and Jarrard DF (2008). Aging and cancer-related loss of

insulin-like growth factor 2 imprinting in the mouse and human prostate. *Cancer Res* **68**, 6797–6802.

[31] Sakatani T, Kaneda A, Iacobuzio-Donahue CA, Carter MG, de Boom Witzel S, Okano H, Ko MS, Ohlsson R, Longo DL, and Feinberg AP (2005). Loss of imprinting of Igf2 alters intestinal maturation and tumorigenesis in mice. *Science* **307**, 1976–1978.

[32] Mathers JC, Strathdee G, and Relton CL (2010). Induction of epigenetic alterations by dietary and other environmental factors. *Adv Genet* **71**, 3–39.

[33] Waterland RA and Jirtle RL (2003). Transposable elements: targets for early nutritional effects on epigenetic gene regulation. *Mol Cell Biol* **23**, 5293–5300.

[34] Saxonov S, Berg P, and Brutlag DL (2006). A genome-wide analysis of CpG dinucleotides in the human genome distinguishes two distinct classes of promoters. *Proc Natl Acad Sci USA* **103**, 1412–1417.

[35] Park JY (2010). Promoter hypermethylation in prostate cancer. *Cancer Control* **17**, 245–255.

[36] Cooper CS and Foster CS (2009). Concepts of epigenetics in prostate cancer development. *Br J Cancer* **100**, 240–245.

[37] Ball MP, Li JB, Gao Y, Lee JH, LeProust EM, Park IH, Xie B, Daley GQ, and Church GM (2009). Targeted and genome-scale strategies reveal gene-body methylation signatures in human cells. *Nat Biotechnol* **27**, 361–368.

[38] Clark SJ (2007). Action at a distance: epigenetic silencing of large chromosomal regions in carcinogenesis. *Hum Mol Genet* **16**, R88–R95.

[39] Truong M, Yang B, Livermore A, Wagner J, Weeratunga P, Huang W, Dhir R, Nelson J, Lin DW, and Jarrard DF (2012). Employing the epigenetic field defect to detect prostate cancer in biopsy-negative patients. *J Urol*, E-pub ahead of print.

Table W1. Clinical and Pathologic Characteristics.

	Methylation Array		Pyrosequencing		
	NTA	TA	NTA	TA	T, TAA, TAD
Number	5	4	12	11	26
Age (years)	63 (55–81)	61 (57–64)	60 (55–70)	59 (51–67)	58 (44–69)
Tumor volume (%)		6.3 (5–10)		5.1 (1–10)	27.1 (5–80)
Gleason grade					
Intermediate		4		11	16
High					10
PSA (ng/ml)		7.7 (4–14)		5.9 (3–14)	6.9 (3–27)

NTA indicates non–tumor-associated normal; PSA, prostate-specific antigen; TA, tumor-associated; T, tumor; TAA, tumor-associated adjacent; TAD, tumor-associated distant; Gleason grade, intermediate: 3 + 3, 3 + 4; high: 4 + 4, 4 + 5, 5 + 5.

Table W2. Primer Sequences.

(A) Pyrosequencing	
CAV1	F—GGGTAATATTTATAAGTTTAATAATAAGGT
	R-biotin—TAAAAACTATCCCAACCCTTC
	Seq—AAGTTTAATAATAAGGTTATGGTAG
EVX1	F—GGAGGAGAGGAAGTTAGGAGTTTATAAAGGA
	R-biotin—CAAATACAACCCAAAACCAAAAACAAT
	Seq—GAAGTTACGAGTTTATAAAGGAT
FGF1	F—GGATGGGATAGTGAAGATAAGAGT
	R-biotin—TTCAACATACTATCATCTAATCCTTTACAC
	Seq—TTTTTTTAAGGTTATGTGATAA
MCF2L	F-biotin—GAGTTGAGTTTTATTTTGGGTATTTTGAAG
	R—ACCCCCAAATTACTAAACTAATATATTCC
	Seq—CAAATTACTAAACTAATATATTCCA
NCR2	F-biotin—GTTGTGGGAGAGTAAGGTTTGGAAATAA
	R—CTCATCTCCACCCCCTTCATTTT
	Seq—CCCCCTTCATTTTCT
WNT2	F—TTTTGGAGGTATAGGGTAGGAAATAA
	R-biotin—AATTCAAAATCATCCAAACCCAAA
	Seq—AGGAAATAATTTTTAATTGAATA
(B) QPCR	
CAV1	F—AACGATGACGTGGTCAAGATTG
	R—TCCAAATGCCGTCAAAACTGT
EVX1	F—AACGCCGAGTACCAGCAC
	R—GTCTCGCTCCCTCCGTTC
FGF1	F—GGAAAGGCTGGAGGAGAACC
	R—TCTGGCCATAGTGAGTCCGA
MCF2L	F—ACCTGTTCCTGCACGAGAAG
	R—ACGGCAGCCATGTTTAAGGA
NCR2	F—TTCCCTCTCCCCAGTCTTCT
	R—GCATCTCACGGTTAGCGTCT
WNT2	F—TAATATGAACGCCCCTCTCG
	R—GCACATTATCGCACATCACC

F indicates forward primer; R, reverse primer; biotin, biotinylated primer; Seq, pyrosequencing primer.

Table W3A. Methylation Peak Locations.

Chromosome	Peak No.	Start Position	End Position
Chr1	1	149471274	149471513
	2	149528409	149528518
	3	149545855	149546294
	4	149623022	149623181
	5	149808643	149809297
Chr2	1	220090490	220090769
	2	234377845	234378894
Chr4	1	118965488	118965968
Chr5	1	131352045	131352509
	2	131353542	131353876
	3	131662526	131662635
	4	131738235	131738344
	5	132044542	132044702
	6	132137727	132138031
	7	132191345	132191874
	8	132192955	132193244
	9	142028596	142029130
	10	142231413	142231596
Chr6	1	41421472	41421891
	2	41426189	41427118
	3	41531833	41531948
	4	41770751	41770870
	5	41799276	41799620
	6	41823331	41823725
	7	73941136	73941485
Chr7	1	27249867	27250156
	2	27329287	27329461
	3	89900634	89901018
	4	115953729	115954078
	5	116053599	116054133
	6	116730563	116730672
	7	126095419	126095629
Chr8	1	118892676	118892958
	2	118981490	118981574
	3	119332465	119332799
Chr9	1	130735749	130735968
	2	130748357	130749031
	3	131036065	131036459
	4	131077814	131077910
	5	131199253	131199592
Chr11	1	1719582	1720442
	2	1892487	1892861
	3	2031460	2031576
	4	2254238	2254517
	5	5400317	5400471
	6	5505469	5505573
	7	64136767	64137036
	8	64140349	64140643
	9	64165697	64165796
	10	64220022	64220131
	11	64223122	64223231
	12	116094656	116104386
	13	116134115	116134214
	14	130699599	130699723
	15	130824509	130824633
	16	131058349	131058948
Chr13	1	29419683	29419977
	2	29488197	29488651
	3	29495438	29495592
	4	112366570	112366660
Chr14	1	53173801	53173890
	2	98498457	98498806
	3	98826247	98826826
	4	98862101	98870359
	5	98917892	98918201
Chr15	1	41601343	41601642
	2	41602618	41603052
	3	41879980	41880329
	4	41897310	41897496
	5	41952848	41953161
	6	41960097	41960426
	7	41991646	41991872
Chr16	1	45572	46086
	2	446846	467671

Table W3A. (*continued*)

Chromosome	Peak No.	Start Position	End Position
Chr18	1	24184165	24184600
	2	59588293	59588522
	3	59788616	59788830
	4	59821299	59821403
Chr19	1	59095365	59095885
	2	59322652	59323121
	3	59334890	59335125
	4	59343796	59344085
	5	59348570	59358710
	6	59448338	59448582
	7	59513349	59513583
	8	59523587	59523836
	9	59558462	59558551
	10	59743846	59744908
	11	59745418	59745535
Chr20	1	33524449	33524913
	2	33552909	33553188
	3	33564800	33565739
	4	33597765	33597993
	5	33603054	33603485
	6	33634685	33634899
	7	33668975	33669309
	8	33677193	33677370
	9	33682853	33682942
Chr21	1	33176986	33177105
	2	34182551	34182660
	3	34278040	34278284
	4	34281522	34282041
	5	39265487	39265596
	6	39409185	39409589
Chr22	1	30438680	30438779
	2	30631862	30632071
	3	30640190	30640309
	4	30699213	30699682
	5	31192667	31192831
	6	31254314	31254964
	7	31286769	31286943
	8	31407471	31408425

Table W3B. Methylated Loci Not Related to Genes.

Location	Hypomethylation or Hypermethylation
Chr1: 149622432–149622488	Hypo
Chr1: 149623022–149623071	Hypo
Chr1: 149709551–149709600	Hypo
Chr2: 234378610–234378659	Hypo
Chr4: 118792613–118792662	Hyper
Chr5: 131617349–131617398	Hypo
Chr5: 132193075–132193124	Hypo
Chr6: 41823506–41823556	Hypo
Chr6: 41823631–41823687	Hypo
Chr7: 27241669–27241718	Hyper
Chr7: 289900969–89901018	Hypo
Chr9: 131077859–131077910	Hypo
Chr11: 1754652–1754701	Hypo
Chr11: 116103872–116103921	Hypo
Chr11: 116103927–116103976	Hypo
Chr11: 116104277–116104326	Hypo
Chr11: 130699674–130699723	Hypo
Chr13: 29419753–29419802	Hypo
Chr13: 29495438–29495487	Hypo
Chr13: 112589940–112589989	Hyper
Chr14: 53173801–53173850	Hypo
Chr14: 98826247–98826296	Hypo
Chr14: 98862411–98862460	Hypo
Chr15: 41878131–41878180	Hyper
Chr15: 41879095–41879145	Hypo
Chr16: 46697–46746	Hypo
Chr18: 24020017–24020072	Hypo
Chr18: 24184165–24184221	Hypo
Chr18: 59906729–59906778	Hypo
Chr20: 33564800–33564852	Hypo
Chr21: 32827756–32827805	Hypo
Chr21: 32869578–32869627	Hyper
Chr21: 33434061–33434110	Hypo
Chr21: 34265892–34265949	Hypo
Chr21: 34281627–34281676	Hypo
Chr21: 34281992–34282041	Hypo
Chr21: 39409540–39409589	Hypo
Chr22: 31056173–31056222	Hypo

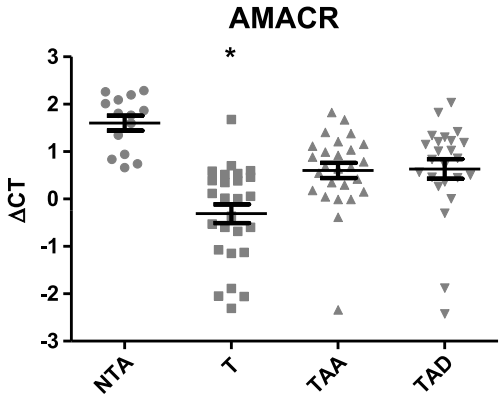

Figure W1. AMACR expression in NTA, T, TAA, and TAD prostate tissues. AMACR is a specific marker expressed by PCa and premalignant lesions. AMACR expression was assayed using RT-QPCR and the data are shown as ΔC_T. On the basis of the above data, two NTA and three TA (T, TAA, and TAD) were excluded from the experiential group due to higher AMACR expression ($P < .05$).

Table W4. Methylation Percentage of All Analyzed CpGs for Each Gene in Microdissected Prostate Specimens.

NTA	TAA	TAD
CAV1		
4.5*	8.8†	9.6†
14.6	22.4†	21.3†
17.8	27.7†	25.8†
13.8	24.3†	23.0†
15.3	25.0†	21.9†
14.9	27.2†	26.4†
18.9	28.0†	26.0
8.3	15.4†	14.7†
15.8	22.7	19.5
17.9	26.7†	28.6†
EVX1		
30.5	38.8†	32.6
28.2	36.9†	29.9
22.7	30.8†	27.8†
50.4	55.4	48.3
46.5	51.7	47.2
36.7	44.8†	40.6†
MCF2L		
80.2	85.2†	85.3†
77.0	85.3†	85.1
96.3	97.4†	96.5
84.8	82.1	80.7†
79.9	86.1	87.5†
FGF1		
80.4	70.7†	70.8†
71.7	60.7†	59.8†
71.2	60.2†	60.9†
81.1	72.9†	71.1†
‡NCR2		
54.3	50.8	52.1
74.7	68.6†	70.7
WNT2		
95.4	89.8†	89.8†
94.9	91.0†	91.5†
100	99.5	100

*CG sites listed in order.
†$P < .05$.
‡High-grade tumor only.

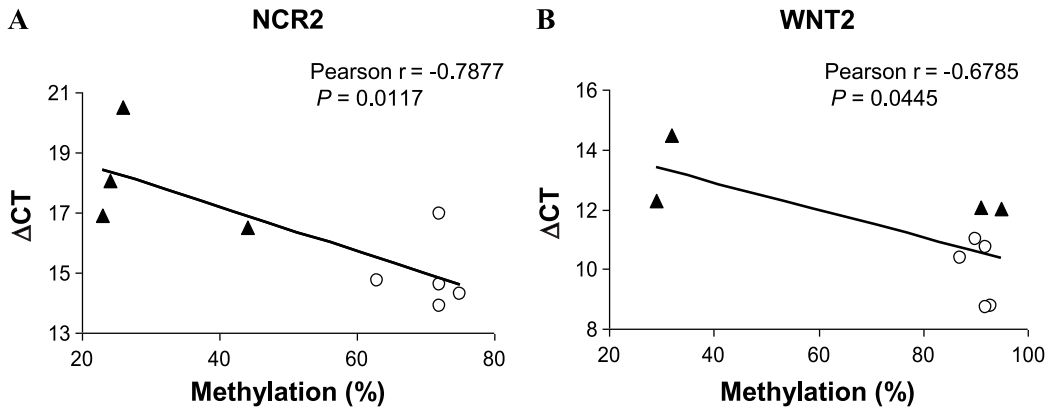

Figure W2. Correlation analysis between methylation and expression at significant loci. Primary cultured normal human prostate epithelial cells (five) were compared to human PCa cell lines (PC3, PPC1, Du145, and LNCaP). DNA methylation was evaluated by pyrosequencing, and gene expression was measured by RT-QPCR and normalized to β-actin (ΔC_T) as described in Materials and Methods section. Loci tested included *CAV1*, *EVX1*, *MCF2L*, and *FGF1* and the two loci only found to be altered in high-grade cancer (*NCR2* and *WNT2*). Only *NCR2* (A) and *WNT2* (B) demonstrated significant alterations in expression between the two groups. In general, significant loci were not located in CpG-enriched promoter regions. A Pearson coefficient was used to demonstrate significant correlations between methylation and expression (●, human prostate epithelial cells; ▲, PCa cell lines; $P < .05$; experiments performed in duplicate).